Hindawi Publishing Corporation
Journal of Nanomaterials
Volume 2015, Article ID 979543, 8 pages
http://dx.doi.org/10.1155/2015/979543

Research Article

CO and C_3H_8 Sensitivity Behavior of Zinc Antimonate Prepared by a Microwave-Assisted Solution Method

Héctor Guillen-Bonilla,[1] Verónica-M. Rodríguez-Betancourtt,[1] José-Trinidad Guillén-Bonilla,[2] Juan Reyes-Gómez,[3] Lorenzo Gildo-Ortiz,[3] Martín Flores-Martínez,[1] M. de la L. Olvera-Amador,[4] and Jaime Santoyo-Salazar[5]

[1]*Departamento de Ingeniería de Proyectos, CUCEI, Universidad de Guadalajara, 44410 Guadalajara, JAL, Mexico*
[2]*Departamento de Electrónica y Computación, CUCEI, Universidad de Guadalajara, 44410 Guadalajara, JAL, Mexico*
[3]*Facultad de Ciencias, Universidad de Colima, 28045 Colima, COL, Mexico*
[4]*Departamento de Ingeniería Eléctrica-SEES, Centro de Investigación y de Estudios Avanzados del Instituto Politécnico Nacional, 07360 México, DF, Mexico*
[5]*Departamento de Física, Centro de Investigación y de Estudios Avanzados del Instituto Politécnico Nacional, 07360 México, DF, Mexico*

Correspondence should be addressed to Juan Reyes-Gómez; reyesgj@ucol.mx

Received 21 September 2015; Accepted 1 December 2015

Academic Editor: Hassan Karimi-Maleh

$ZnSb_2O_6$ has been synthesized by a microwave-assisted solution method in order to test its possible application as a gas sensor. Zinc nitrate, antimony trichloride, and ethylenediamine were used as precursors and deionized water as solvent. Microwave radiation, with a power of ~350 W, was applied for solvent evaporation. The thermal decomposition of the precursors leads to the formation of $ZnSb_2O_6$ at 600°C. This oxide crystallized in a tetragonal structure with cell parameters $a = 4.66$ Å, $c = 9.26$ Å and space group $P4_2/mnm$. Microwires and microrods formed by nanocrystals were observed by means of scanning and transmission electron microscopies (SEM and TEM, resp.). Pellets of the oxide were tested as gas sensors in flowing atmospheres of carbon monoxide (CO) and propane (C_3H_8). Sensitivity increased with the gas concentration (0–300 ppm) and working temperatures (ambient, 150 and 250°C) increase. The results indicate high sensitivity of $ZnSb_2O_6$ in both gases at different concentrations and operating temperatures.

1. Introduction

The need of reliable detection devices for dangerous atmospheres has promoted a huge research since past decades on the development of semiconductor materials suitable as gas sensors. In general, the gas sensors are used in domestic applications and industrial processes like monitoring of automobile exhaust gases, flue-gases in incinerators, the possible toxicity in the air, and so forth [1–5]. Important criteria for the fabrication of these sensors are low price, chemical stability, selectivity, and very good sensitivity [6, 7]. Among all semiconductors that can be used as sensors, the binary oxide SnO_2 is regarded as one of the most promising materials for such purpose [8–11], because it possesses some of the above desired features, like high sensitivity and chemical stability [12–14]. However, some other semiconductor types, with more complex crystal structures, are currently investigated, like the ones with perovskite structure: $Ca_xPb_{1-x}TiO_3$, $SmFeO_3$, and $SrFeO_3$ [15–17]; spinel structure: $MgAl_2O_4$, $CdCr_2O_4$, and $ZnFe_2O_4$ [18–20]; and oxides with trirutile-type structure: $CoTa_2O_6$, $NiTa_2O_6$, and $CoSb_2O_6$ [21–23]. Among the latter, the type-n semiconductor zinc antimonate $ZnSb_2O_6$ has been extensively studied for gas sensing applications due to its high response to several toxic gases [24]. Our work presented here is devoted to such material.

Michel et al. [25] synthesized $ZnSb_2O_6$ through a colloidal method and probed its sensing capabilities in O_2, CO, and CO_2 atmospheres by means of dynamic tests using

frequencies from 0.1 to 100 kHz at a temperature of 400°C. Their results showed good selectivity, reproducibility, and chemical stability. Tamaki et al. [26] prepared thick films of $ZnSb_2O_6$ through a dip-coating method, obtaining good selectivity and stability in H_2S atmospheres, attributing this to the film's porous structure.

Generally speaking, the zinc antimonate adopts a formula ASb_2O_6, where A can be substituted by the divalent Zn ion or the ions Ni, Co, Mg, and Cu, among others [27]. This oxide belongs to the family of trirutile-type materials and crystallizes in a tetragonal structure with a space group $P4_2/mnm$ [28]. In general, the trirutile-type materials are synthesized by a ceramic-method [29] but $ZnSb_2O_6$ has been better prepared by a colloidal-route [25]. In our work, we synthesized the oxide through a microwave-assisted solution-method and prepared pellets with it in order to test its sensing capabilities in CO and C_3H_8 atmospheres at relative low temperatures.

2. Experimental Procedures

2.1. Synthesis of $ZnSb_2O_6$. We synthesized $ZnSb_2O_6$ preparing three solutions: 1.48 g (0.005 mol) of $Zn(NO_3)_2{\cdot}6H_2O$ (J. T. Baker), 2.28 g (0.01 mol) of $SbCl_3$ (Sigma-Aldrich), and 0.5 mL of ethylenediamine (Sigma), dissolving each separately in 5 mL of distilled water. The solutions were magnetically stirred at 350 rpm during 20 min. After that, the antimony chloride and ethylenediamine solutions were mixed under stirring. The zinc nitrate solution was next slowly poured to the mixed solution under stirring at 350 rpm during 24 h. After this, the solvent was evaporated by means of fourteen 180 s-microwave-exposures at ~350 W (General Electric microwave oven, model JES769WK; the absorbed energy was estimated to 863 kJ), recording a temperature of ~92°C after each exposure. Temperature and exposure time were controlled in order to avoid material loss by splashing. After the evaporation, the product was heated at 200°C during 8 h and afterward calcined in air at 600°C during 5 h with a heat rate of 100°C/h using a temperature-controlled oven (Vulcan 3-550).

2.2. Physical Characterization of $ZnSb_2O_6$ Powders. The synthesized zinc antimonate ($ZnSb_2O_6$) powders were analyzed by means of X-ray diffraction (Siemens D 500 XRD-system, CuKα radiation, 2θ scanning-angle from 10 to 70° and 1-second steps of 0.02°). The powders were analyzed by Raman spectroscopy using a 1000B microRaman Renishaw system, calibrated with a silicon semiconductor with its characteristic Raman peak at 520 cm^{-1}. The laser (excitation wavelength of 830 nm) was focused on the surface of the powders (spot size of approximately 20 μm) by means of a Leica optical microscope (DMLM) integrated to the microRaman system. The radiation energy on the sample was 4.5 mW during 60 s. The microstructure was analyzed by means of scanning electron microscopy (JEOL JSM-6390LV SEM-system, in high-vacuum mode, using secondary-electron-emission) and a dispersion in isopropyl alcohol of the powders was put in a copper grid and analyzed by means of transmission electron microscopy (JEOL JEM-2010 TEM-system, at a 200 kV accelerating voltage).

2.3. Pellets Preparation for Gas Sensitivity Analysis. For the sensitivity studies, pellets from the calcined powders were prepared using 0.353 g of them and compressed by means of a 25-ton manual-pressing-equipment (SIMPLEX ITAL EQUIP). The best pressing parameters were 20 tons during 120 min, obtaining pellets with a diameter of 12 mm, and a thickness of 500 μm.

The pellets of $ZnSb_2O_6$, with a thickness of 500 μm, were exposed to carbon monoxide (CO) and propane (C_3H_8) flows at concentrations 5, 50, 100, 200, and 300 ppm of both gases. Working temperatures were 23°C (ambient), 150°C, and 250°C. The sensitivity changes (S) were evaluated using [30–32]

$$S = \frac{G_G - G_O}{G_O}, \tag{1}$$

where G_G and G_O are electrical conductance of the $ZnSb_2O_6$ pellets measured in gas (CO or C_3H_8) and air, respectively.

For this analysis, a measuring vacuum chamber with a vacuum capacity of 10^{-3} Torr was used. Gas concentration and partial pressure were controlled using a TM20 Leybold detector. Electric resistance measures were carried out by means of a digital multimeter (model Keithley 2001). See Figure 1.

3. Results and Discussion

3.1. XRD Analysis. Figure 2 shows a diffractogram depicting the zinc antimonate ($ZnSb_2O_6$) oxide's peaks corresponding to the different crystal planes, which were identified by means of the JCPDF file 38-0453. It was found that the oxide exhibits a tetragonal crystal structure with cell parameters a = 4.66 Å, c = 9.26 Å and a $P4_2/mnm$ spatial group. That means the oxide is a trirutile phase type [24, 26, 33, 34], which agrees with the results in [35, 36]. Furthermore, the small peaks at 2θ = 29.62°, 42.54°, and 60.61° belong to the secondary phase $ZnSb_2O_4$ [25], which were identified through the JCPDF file 15-0802.

In previous works, the $ZnSb_2O_6$ oxide has been prepared through different synthesis routes, obtaining the oxide generally above a temperature of 600°C. For example, Wu et al. [37] prepared the oxide by means of a solid-state-reaction, mixing ZnO and Sb_2O_3 at 700–1000°C, and Zhu et al. [38] used the vapor-phase-oxidation method in a Ar + O_2 atmosphere at a temperature between 500 and 900°C. In the present work, the synthesis of the oxide by means of a microwave-assisted solution method was done at a temperature of 600°C, which brings some advantages against the previously cited works.

3.2. Raman Spectroscopy Analysis. The Raman spectrum of the oxide is depicted in Figure 3, where the main bands ν_7 to ν_{10}, in the range 500–800 cm^{-1}, correspond to the vibration of the Sb_2O_{10} units of the oxide's crystals, and the weaker bands ν_1 to ν_6, which are below 400 cm^{-1}, are due to the influence of Zn^{2+}. In more detail, in the range 600–800 cm^{-1}, the stretching modes of the Sb–O_p bonds predominate, while

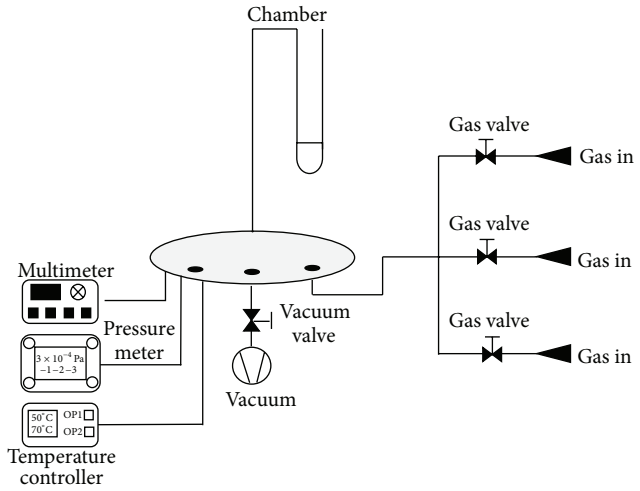

Figure 1: Experimental array for the sensitivity testing of $ZnSb_2O_6$.

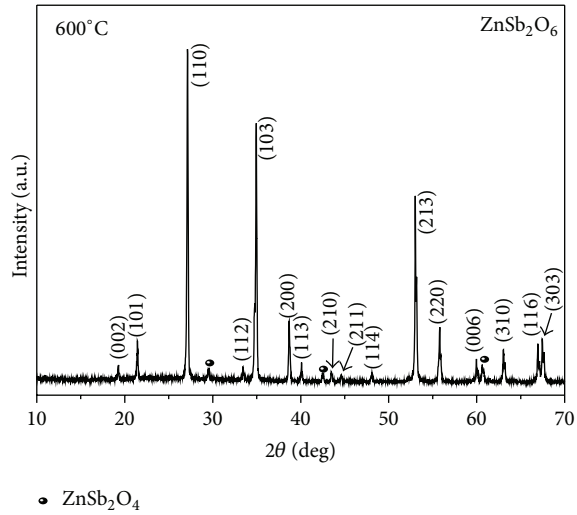

Figure 2: Diffractogram of the zinc antimonate ($ZnSb_2O_6$) powders calcined at 600°C in air.

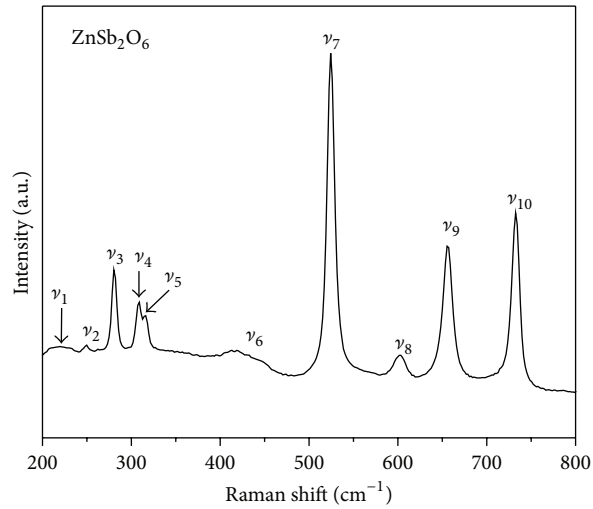

Figure 3: Raman spectrum of the $ZnSb_2O_6$ powders calcined at 600°C in air.

in the range 400–500 cm^{-1}, the deformation modes of the Sb–O_p bonds, coupled to the vibrations of the Zn–O bonds, are dominant. The 500–600 cm^{-1} bands are due to the elongation modes of the Sb–O_{cyc} bonds [39, 40]. This analysis supports the results obtained by XRD, shown above.

3.3. Scanning Electron Microscopy Analysis. Figure 4 shows three typical SEM photomicrographs of trirutile-type zinc antimonate ($ZnSb_2O_6$) powders after calcination at 600°C. These images present three different magnifications: 100x, 500x, and 1500x.

A dendrite-like formation of microwires and microrods is depicted in Figure 4(a), at 100x (see the inserted zoom), which can be due to the rise of the temperature during the calcinations, the lasted time by the material in the muffle, and the ethylenediamine concentration [41]. About the latter, the ethylenediamine incorporates into the organic frame and then escapes as a result of the thermal treatment, giving rise to the desired morphologies, like those obtained in this work. The importance of ethylenediamine in the formation of nano- and microstructures has been discussed in previous works [42, 43]. In our case, the microrod's length was estimated in the range 10–100 μm with a standard deviation of 21.3 μm and an average of 59.5 μm. The averaged diameter was of 1.5 μm (see Figure 4(b)). As can be observed, tiny crystals (average size of 1.1 μm) agglomerate to give shape to the microrods. At 1500x (Figure 4(c)), more details of the microstructure can be seen, where a porous surface and the strong agglomeration of individual particles, with irregular shape, are clearly discernible. The agglomeration is due to the formation of necks caused by the elimination of organic material after the thermal treatment. The porosity is attributed to the release of gases during the thermal decomposition, mainly water vapor, NO_x, and CO_2 [31, 44].

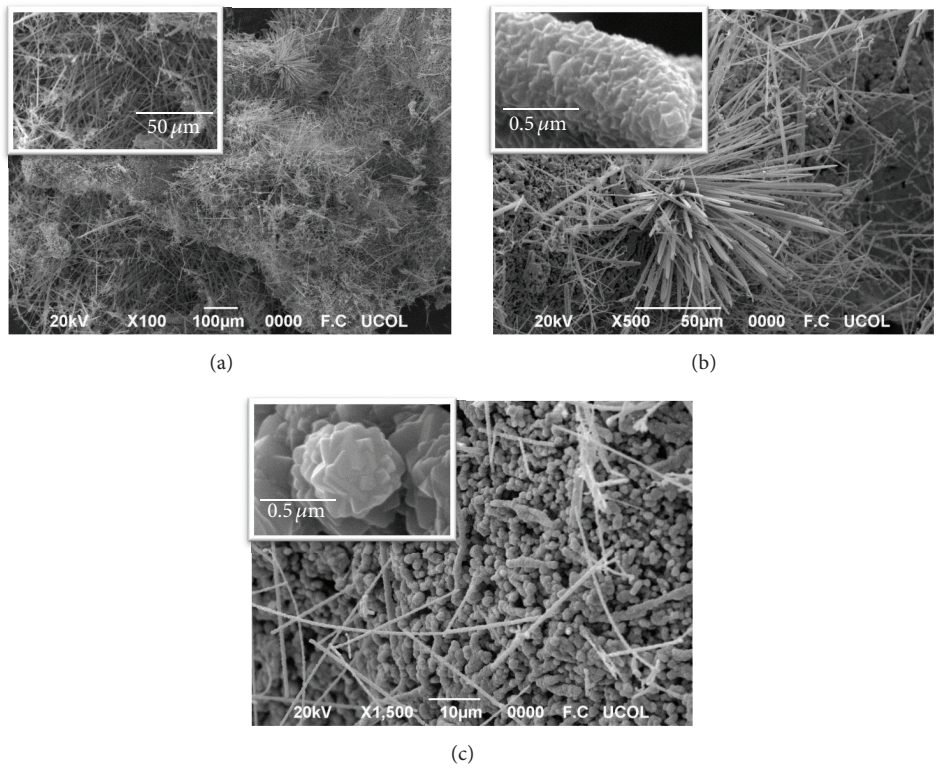

Figure 4: SEM images of trirutile-type zinc antimonate ($ZnSb_2O_6$) powders calcined at 600°C at different magnifications: (a) 100x, (b) 500x, and (c) 1500x.

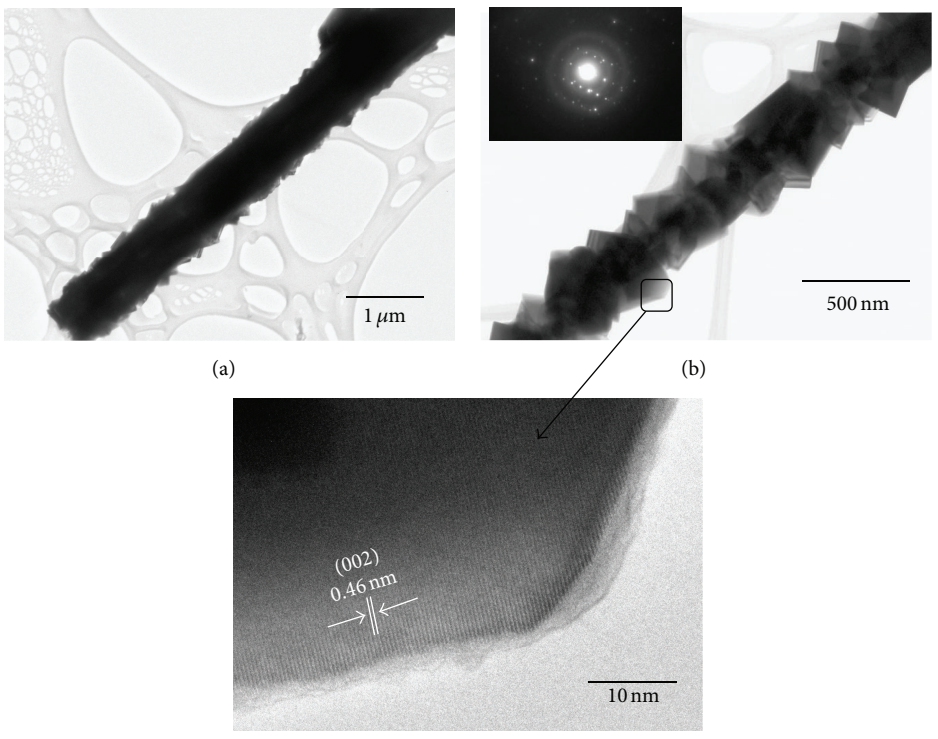

Figure 5: TEM analysis of trirutile-type zinc antimonate ($ZnSb_2O_6$) powders (600°C): ((a), (b)) microrods formed by crystals, (c) HRTEM image showing the lattice fringes.

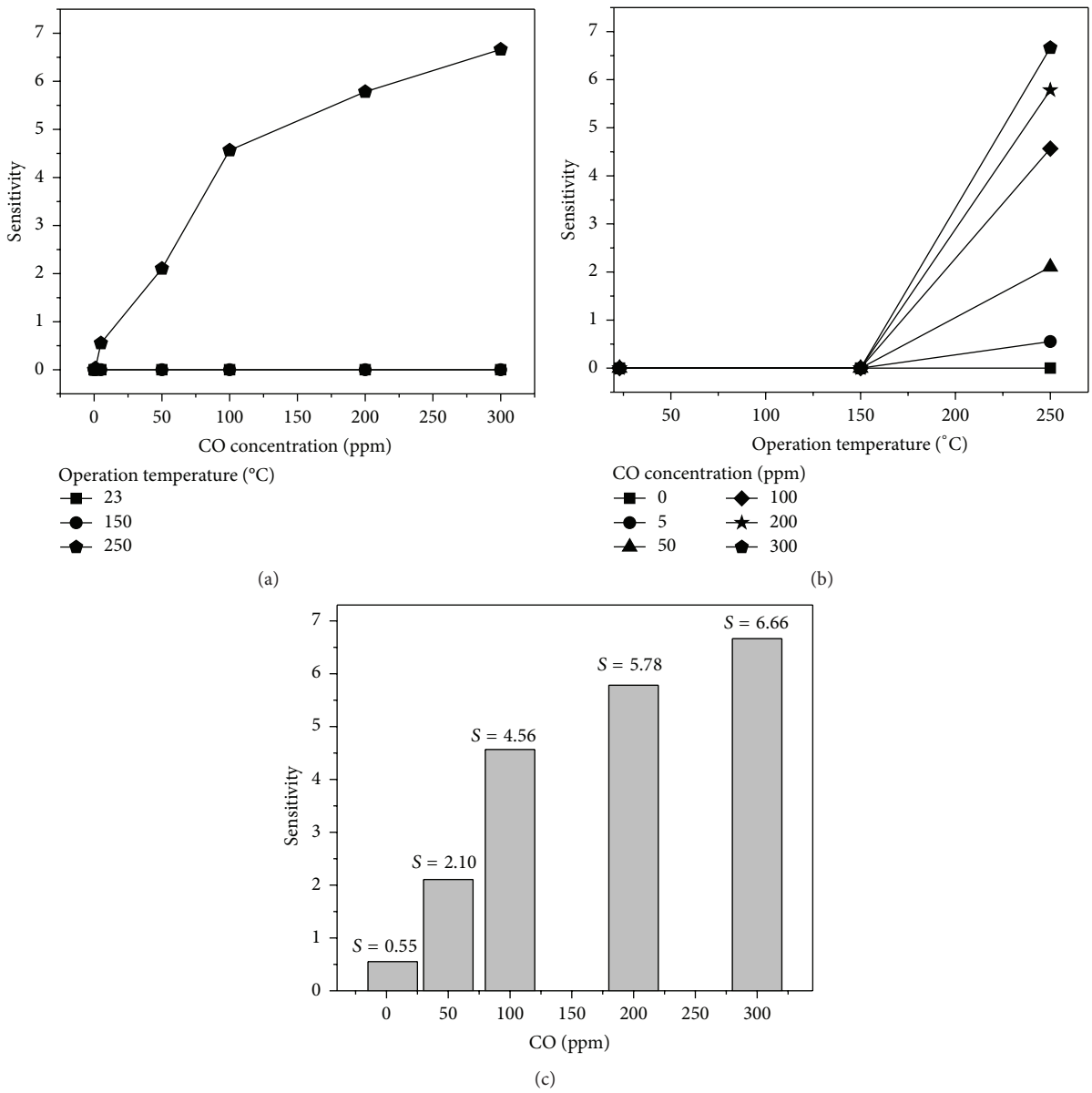

Figure 6: Sensitivity of $ZnSb_2O_6$ pellets as a function of (a) CO concentration and (b) CO operating temperature; (c) maximum values of S at 250°C for every CO concentration.

3.4. Transmission Electron Microscopy Analysis. Figure 5 shows typical images obtained by transmission electron microscopy. In Figures 5(a) and 5(b) photomicrographs of the microrods formed by the tiny cubic-shaped crystals can be observed. The analyzed microrod in Figure 5(a) had a length of 6.6 μm and a diameter of 0.857 μm, while the tiny crystal's size was around 50–250 nm (Figure 5(b)). High resolution transmission electron microscopy (HRTEM) was performed in a selected zone of the sample (Figures 5(b) and 5(c)). The HRTEM image reveals that the interplanar distance is around 0.46 nm, which corresponds to (002) planes. In order to verify the local crystallinity of the sample, selected area electron diffraction (SAED) was made on several rods. The inset in Figure 5(b) shows a typical pattern; these results confirmed the crystallinity of the sample previously registered in XRD analysis.

3.5. Sensing Properties. The variations of the sensitivity's magnitude are shown in Figures 6(a)–6(c) in carbon monoxide (CO) atmospheres.

These results show that $ZnSb_2O_6$ is highly sensitive to the employed CO concentrations and to operation temperatures above 150°C. No significant variations below such temperature were found. The maximum value of the sensitivity was of ~6.66 for a concentration of 300 ppm at 250°C. The increase of the sensitivities with the concentration is due to the raise of the number of gas molecules, which react with the adsorbed oxygen, donating electrons to the material's surface

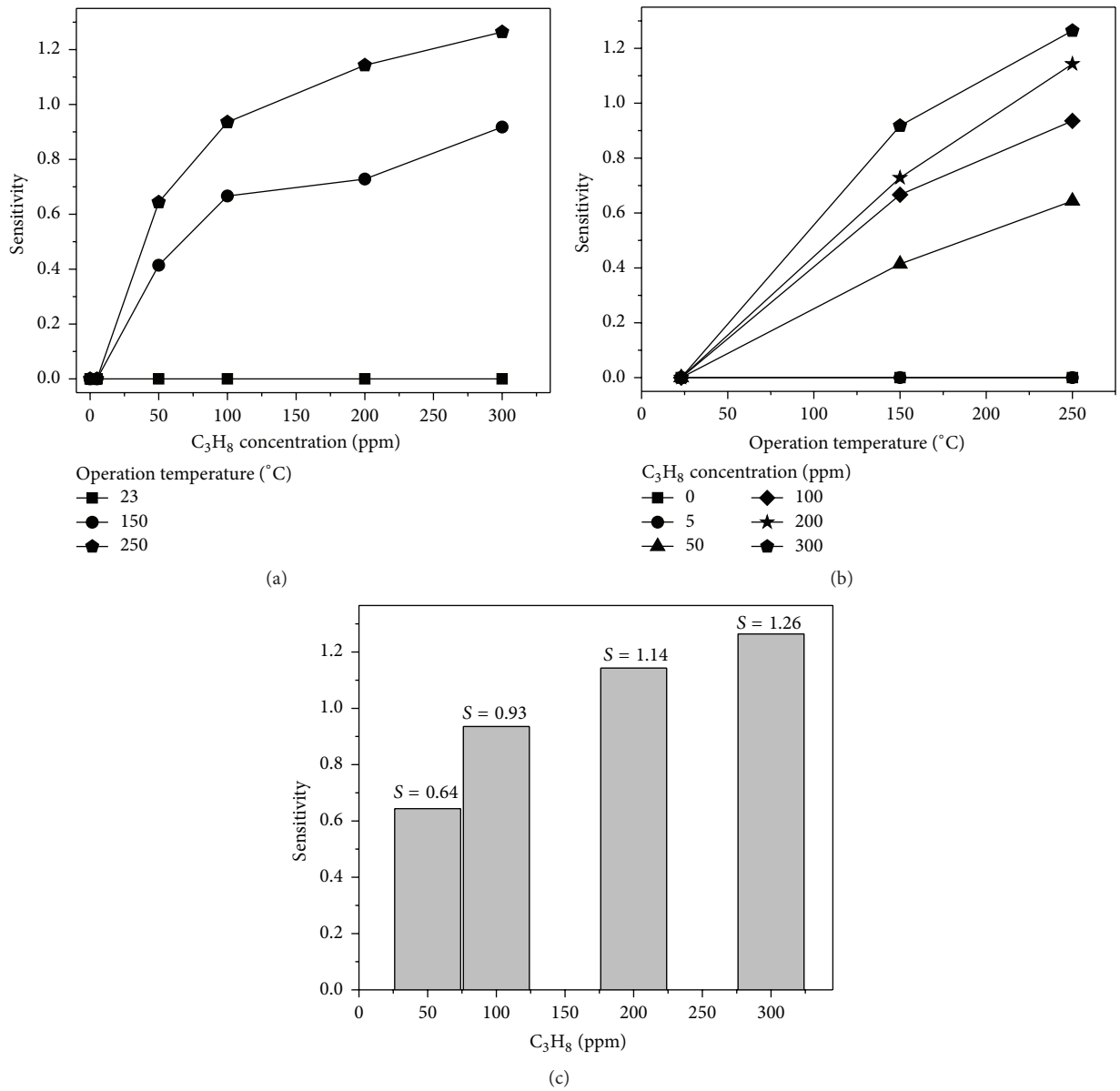

Figure 7: Sensitivity of $ZnSb_2O_6$ pellets as a function of (a) propane (C_3H_8) concentration and (b) operating temperature; (c) maximum values of S at 250°C at different propane concentrations.

[31, 45]. The most accepted mechanism to explain this is a model based on the depletion layer's modulation due to the oxygen adsorption [8, 11, 14]. In this model [14], the adsorbed oxygen on the semiconductor's surface ionizes to O^- and O^{2-}, diminishing consequently the carriers concentration and the electrons' mobility, because these species are more reactive than others (like O_2^-, which is not produced or is detected because the thermal energy is not enough for that) at temperatures above 150°C [46]. $ZnSb_2O_6$ strongly reacts above such temperature with CO [31, 32] of the atmosphere yielding CO_2 and releasing electrons back into the conduction band [25, 47], especially at the temperature of 250°C, producing a high sensitivity.

A similar trend was found for different propane concentrations and operation temperatures (Figures 7(a)–7(c)). As expected, at ambient temperature (23°C) no variation of the sensitivity was detected, but when the temperature was increased, sensitivity variations were observed. The maximum was $S \sim 1.26$ at 250°C for a propane concentration of 300 ppm. A mechanism to explain the propane detection at relative low temperatures, like 250°C or 350°C, has not been yet reported. Other investigations, using similar semiconductor oxides (like SnO_2 and ZnO) to detect propane, report a maximum sensitivity of ~0.7 and ~0.6 for a propane concentration of 500 ppm at 300°C [48, 49]. Comparatively, we obtained better results here. In addition, we have found in previous works, using a cobalt oxide in the same atmospheres, that a trirutile-type structure, like that of the oxide of this work, is highly responsible for a great performance and excellent stability [32].

4. Conclusions

Zinc antimonate ($ZnSb_2O_6$), with a trirutile-type structure, forming microstructures like microrods and microwires and intended to be used for gas sensing applications, was successfully synthesized employing a microwave-assisted solution-method at relative low temperatures. Tested pellets of $ZnSb_2O_6$ were clearly sensitive and uniform in response to the operating temperatures and gas concentrations in carbon monoxide (CO) and propane (C_3H_8) atmospheres. A good sensitivity was obtained at 250°C, with a maximum $S = 6.66$ (CO) and $S = 1.2$ (C_3H_8) at 300 ppm. It has been found that $ZnSb_2O_6$ is a strong candidate for being applied as an environmental gas sensor.

Conflict of Interests

The authors declare that there is no conflict of interests regarding the publication of this paper.

Acknowledgments

Héctor Guillen-Bonilla acknowledges Mexico's *Consejo Nacional de Ciencia y Tecnología* (CONACyT) for the received financial support. The technical support received from Darío Pozas Zepeda and Miguel Ángel Luna Arias is also appreciated. This work was partially supported by Project no. 263656 from CONACyT, Project no. 254790 from CONACyT, and Project no. 784-12 FRABA.

References

[1] M. Fleischer and H. Meixner, "Fast gas sensors based on metal oxides which are stable at high temperatures," *Sensors and Actuators B: Chemical*, vol. 43, no. 1–3, pp. 1–10, 1997.

[2] N. D. Hoa, N. V. Duy, S. A. El-Safty, and N. V. Hieu, "Meso-/nanoporous semiconducting metal oxides for gas sensor applications," *Journal of Nanomaterials*, vol. 2015, Article ID 972025, 14 pages, 2015.

[3] C. J. Belle, A. Bonamin, U. Simon et al., "Size dependent gas sensing properties of spinel iron oxide nanoparticles," *Sensors and Actuators, B*, vol. 160, no. 1, pp. 942–950, 2011.

[4] K. Arshak and I. Gaidan, "Development of a novel gas sensor based on oxide thick films," *Materials Science and Engineering: B*, vol. 118, no. 1–3, pp. 44–49, 2005.

[5] W. Chen, H. Gan, W. Zhang, and Z. Mao, "Hydrothermal synthesis and hydrogen sensing properties of nanostructured SnO_2 with different morphologies," *Journal of Nanomaterials*, vol. 2014, Article ID 291273, 7 pages, 2014.

[6] M.-I. Baraton and L. Merhari, "Electrical behavior of semiconducting nanopowders versus environment," *Reviews on Advanced Materials Science*, vol. 4, no. 1, pp. 15–24, 2003.

[7] N. Yamazoe, "Toward innovations of gas sensor technology," *Sensors and Actuators B: Chemical*, vol. 108, no. 1-2, pp. 2–14, 2005.

[8] G. Sberveglieri, "Recent developments in semiconducting thin-film gas sensors," *Sensors and Actuators B: Chemical*, vol. 23, no. 2-3, pp. 103–109, 1995.

[9] A. Licciulli, S. Mazzarelli, G. De, P. Siciliano, L. Vasanelli, and R. Rella, "Os and Pd modified tin oxide films for sensors by the sol gel process," *Journal of Sol-Gel Science and Technology*, vol. 21, no. 3, pp. 195–201, 2001.

[10] S. Nicoletti, L. Dori, F. Corticelli, M. Leoni, and P. Scardi, "Tin oxide thin-film sensors for aromatic hydrocarbons detection: effect of aging time on film microstructure," *Journal of the American Ceramic Society*, vol. 82, no. 5, pp. 1201–1206, 1999.

[11] M. Hübner, C. E. Simion, A. Haensch, N. Barsan, and U. Weimar, "CO sensing mechanism with WO_3 based gas sensors," *Sensors and Actuators, B: Chemical*, vol. 151, no. 1, pp. 103–106, 2010.

[12] G. Martinelli and M. C. Carotta, "Thick-film gas sensors," *Sensors and Actuators B: Chemical*, vol. 23, no. 2-3, pp. 157–161, 1995.

[13] M. Yuasa, T. Masaki, T. Kida, K. Shimanoe, and N. Yamazoe, "Nano-sized PdO loaded SnO_2 nanoparticles by reverse micelle method for highly sensitive CO gas sensor," *Sensors and Actuators B: Chemical*, vol. 136, no. 1, pp. 99–104, 2009.

[14] T. Zhang, L. Liu, Q. Qi, S. Li, and G. Lu, "Development of microstructure In/Pd-doped SnO_2 sensor for low-level CO detection," *Sensors and Actuators B: Chemical*, vol. 139, no. 2, pp. 287–291, 2009.

[15] L. Jingbo, L. Wenchao, Z. Yanxi, and W. Zhimin, "Preparation and characterization of Li^+-modified $Ca_xPb_{1-x}TiO_3$ film for humidity sensor," *Sensors and Actuators B: Chemical*, vol. 75, no. 1-2, pp. 11–17, 2001.

[16] M. C. Carotta, G. Martinelli, Y. Sadaoka, P. Nunziante, and E. Traversa, "Gas-sensitive electrical properties of perovskite-type $SmFeO_3$ thick films," *Sensors and Actuators B: Chemical*, vol. 48, no. 1-3, pp. 270–276, 1998.

[17] Y. Wang, J. Chen, and X. Wu, "Preparation and gas-sensing properties of perovskite-type $SrFeO_3$ oxide," *Materials Letters*, vol. 49, no. 6, pp. 361–364, 2001.

[18] V. Coillard, H. Debéda, C. Lucat, and F. Ménil, "Nitrogen monoxide detection with a planar spinel coated amperometric sensor," *Sensors and Actuators B*, vol. 78, no. 1–3, pp. 113–118, 2001.

[19] G. Lu, N. Miura, and N. Yamazoe, "A high temperature amperometric NO sensor based on stabilized zirconia and $CdCr_2O_4$ electrode," *Journal of Applied Electrochemistry*, vol. 28, no. 9, pp. 1009–1011, 1998.

[20] Y. Shimizu, S. Kusano, H. Kuwayama, K. Tanaka, and M. Egashira, "Oxygen-sensing properties of spinel-type oxides for stoichiometric air/fuel combustion control," *Journal of the American Ceramic Society*, vol. 73, no. 4, pp. 818–824, 1990.

[21] P. T. Moseley, D. E. Williams, J. O. W. Norris, and B. C. Tofield, "Electrical conductivity and gas sensitivity of some transition metal tantalates," *Sensors and Actuators*, vol. 14, no. 1, pp. 79–91, 1988.

[22] C. R. Michel, H. Guillén-Bonilla, A. H. Martínez-Preciado, and J. P. Morán-Lázaro, "Synthesis and gas sensing properties of nanostructured $CoSb_2O_6$ microspheres," *Sensors and Actuators B: Chemical*, vol. 143, no. 1, pp. 278–285, 2009.

[23] A. Guillén-Bonilla, V.-M. Rodríguez-Betancourtt, M. Flores-Martínez et al., "Dynamic response of $CoSb_2O_6$ trirutile-type oxides in a CO_2 atmosphere at low-temperatures," *Sensors*, vol. 14, no. 9, pp. 15802–15814, 2014.

[24] N. Kikuchi, H. Hosono, H. Kawazoe, O. Tanegashima, I. Ota, and Y. Kimura, "Carrier generation in wide-gap conductor, zinc antimonate," *Journal of the American Ceramic Society*, vol. 88, no. 10, pp. 2793–2797, 2005.

[25] C. R. Michel, N. L. López Contreras, M. A. López-Alvarez, and A. H. Martínez-Preciado, "Gas selectivity of nanostructured

$ZnSb_2O_6$ synthesized by a colloidal method," *Sensors and Actuators B: Chemical*, vol. 171-172, pp. 686–690, 2012.

[26] J. Tamaki, Y. Yamada, Y. Yamamoto, M. Matsuoka, and I. Ota, "Sensing properties to dilute hydrogen sulfide of $ZnSb_2O_6$ thick-film prepared by dip-coating method," *Sensors and Actuators B: Chemical*, vol. 66, no. 1, pp. 70–73, 2000.

[27] E. Husson, Y. Repelin, and H. Brusset, "Comparaison des champs de force des niobates, tantalates et antimoniates de structure columbite et trirutile," *Journal of Solid State Chemistry*, vol. 33, no. 3, pp. 375–384, 1980.

[28] E. Filipek and G. Dąbrowska, "Unknown thermal properties of $ZnSb_2O_6$ and $Zn_7Sb_2O_{12}$ compounds: reactivity of α-Sb_2O_4 with ZnO on heating in air," *Journal of Thermal Analysis and Calorimetry*, vol. 94, no. 1, pp. 195–201, 2008.

[29] D. Larcher, A. S. Prakash, L. Laffont et al., "Reactivity of antimony oxides and MSb_2O_6 (M = Cu, Ni, Co), trirutile-type phases with metallic lithium," *Journal of the Electrochemical Society*, vol. 153, no. 9, pp. A1778–A1787, 2006.

[30] G. Carbajal-Franco, A. Tiburcio-Silver, J. M. Domínguez, and A. Sánchez-Juárez, "Thin film tin oxide-based propane gas sensors," *Thin Solid Films*, vol. 373, no. 1-2, pp. 141–144, 2000.

[31] L. Gildo-Ortiz, H. Guillén-Bonilla, J. Santoyo-Salazar et al., "Low-temperature synthesis and gas sensitivity of perovskite-type $LaCoO_3$ nanoparticles," *Journal of Nanomaterials*, vol. 2014, Article ID 164380, 8 pages, 2014.

[32] H. Guillén-Bonilla, L. Gildo-Ortiz, M. L. Olvera-Amador et al., "Sensitivity of mesoporous $CoSb_2O_6$ nanoparticles to gaseous CO and C_3H_8 at low temperatures," *Journal of Nanomaterials*, vol. 2015, Article ID 308465, 9 pages, 2015.

[33] M. L. Arefin, F. Raether, D. Dolejš, and A. Klimera, "Phase formation during liquid phase sintering of ZnO ceramics," *Ceramics International*, vol. 35, no. 8, pp. 3313–3320, 2009.

[34] E.-O. Giere, A. Brahimi, H. J. Deiseroth, and D. Reinen, "The geometry and electronic structure of the Cu^{2+} polyhedra in trirutile-type compounds $Zn(Mg)_{1-x}Cu_xSb_2O_6$ and the dimorphism of $CuSb_2O_6$: a solid state and EPR study," *Journal of Solid State Chemistry*, vol. 131, no. 2, pp. 263–274, 1997.

[35] H. Mizoguchi and P. M. Woodward, "Electronic structure studies of main group oxides possessing edge-sharing octahedra: implications for the design of transparent conducting oxides," *Chemistry of Materials*, vol. 16, no. 25, pp. 5233–5248, 2004.

[36] J. Singh, N. Bhardwaj, and S. Uma, "Single step hydrothermal based synthesis of $M(II)Sb_2O_6$ (M = Cd and Zn) type antimonates and their photocatalytic properties," *Bulletin of Materials Science*, vol. 36, no. 2, pp. 287–291, 2013.

[37] S. Wu, G. Li, Y. Zhang, and W. Zhang, "Surface photoelectric and visible light driven photocatalytic properties of zinc antimonate-based photocatalysts," *Materials Research Bulletin*, vol. 48, no. 3, pp. 1117–1121, 2013.

[38] B. L. Zhu, C. S. Xie, A. H. Wang, D. W. Zeng, M. L. Hu, and W. Y. Wang, "Electrical conductivity and gas sensitivity of Zn–Sb–O thick films," *Materials Research Bulletin*, vol. 39, no. 3, pp. 409–415, 2004.

[39] H. Haeuseler, "Infrared and Raman spectra and normal coordinate calculations on trirutile-type compounds," *Spectrochimica Acta Part A: Molecular Spectroscopy*, vol. 37, no. 7, pp. 487–495, 1981.

[40] E. Husson, Y. Repelin, H. Brusset, and A. Cerez, "Spectres de vibration et calcul du champ de force des antimoniates et des tantalates de structure trirutile," *Spectrochimica Acta Part A*, vol. 35, no. 10, pp. 1177–1187, 1979 (French).

[41] H. Guillén-Bonilla, J. Reyes-Gomez, A. Guillén-Bonilla et al., "Synthesis and characterization of $MgSb_2O_6$ trirutile-type in low presence concentrations of ethylenediamine," *Journal of Chemistry and Chemical Engineering*, vol. 7, pp. 395–401, 2013.

[42] Z.-X. Deng, C. Wang, X.-M. Sun, and Y.-D. Li, "Structure-directing coordination template effect of ethylenediamine in formations of ZnS and ZnSe nanocrystallites via solvothermal route," *Inorganic Chemistry*, vol. 41, no. 4, pp. 869–873, 2002.

[43] X. Wang and Y. Li, "Solution-based synthetic strategies for 1-D nanostructures," *Inorganic Chemistry*, vol. 45, no. 19, pp. 7522–7534, 2006.

[44] C. R. Michel, A. H. Martínez, F. Huerta-Villalpando, and J. P. Morán-Lázaro, "Carbon dioxide gas sensing behavior of nanostructured $GdCoO_3$ prepared by a solution-polymerization method," *Journal of Alloys and Compounds*, vol. 484, no. 1-2, pp. 605–611, 2009.

[45] N. J. Dayan, S. R. Sainkar, R. N. Karekar, and R. C. Aiyer, "Formulation and characterization of ZnO:Sb thick-film gas sensors," *Thin Solid Films*, vol. 325, no. 1-2, pp. 254–258, 1998.

[46] C.-C. Hsiao and L.-S. Luo, "A rapid process for fabricating gas sensors," *Sensors*, vol. 14, no. 7, pp. 12219–12232, 2014.

[47] S. C. Chang, "Oxygen chemisorption on tin oxide: correlation between electrical conductivity and EPR measurements," *Journal of Vacuum Science and Technology*, vol. 17, no. 1, pp. 366–369, 1979.

[48] H. Gómez-Pozos, J. L. González-Vidal, G. A. Torres, M. de la Luz Olvera, and L. Castañeda, "Physical characterization and effect of effective surface area on the sensing properties of tin dioxide thin solid films in a propane atmosphere," *Sensors*, vol. 14, no. 1, pp. 403–415, 2013.

[49] H. Gómez-Pozos, J. L. González-Vidal, G. A. Torres et al., "Chromium and ruthenium-doped zinc oxide thin films for propane sensing applications," *Sensors*, vol. 13, no. 3, pp. 3432–3444, 2013.